Mechanics of Materials 161 (2021) 104006

Contents lists available at ScienceDirect

Mechanics of Materials

journal homepage: www.elsevier.com/locate/mechmat

A multiscale experimental approach to characterize micro-to-macro transition length scale in polymer foams

Behrad Koohbor [a,*], Nicholas Pagliocca [a], George Youssef [b]

[a] Department of Mechanical Engineering, Rowan University, 201 Mullica Hill Rd., Glassboro, NJ, 08028, USA
[b] Experimental Mechanics Laboratory, Department of Mechanical Engineering, San Diego State University, 5500 Campanile Drive, San Diego, CA, 92182, USA

ARTICLE INFO

Keywords:
Multiscale
Homogenization
Representative volume element (RVE)
Digital image correlation
Foam

ABSTRACT

Bridging between micromechanics response and macroscopic behavior is at the core of multiscale investigations in heterogeneous materials. As such, quantitative characterization of the transitional length scales that correlate micro and macroscale behaviors is of great importance. Experimental characterization of the so-called transitional length scales in foams and other cellular structures is extremely scarce. The present work reports on an experimental-statistical approach proposed to quantify the micro-to-macro transition length scale in polymeric foams. The approach proposed in this work uses full-field strain distributions measured by digital image correlation (DIC) at two scales as input. The physical dimensions of the transition length scale are identified by implementing a statistical algorithm based on spatial averaging of the local strain data obtained from DIC. Interestingly, the transition between micro and macroscale deformation is found to be a function of material density but independent of global strain and stresses applied. The present results provide direct validations to representative volume element (RVE) size in cellular solids determined by computational methods.

1. Introduction

Foams are an essential class of engineering materials that have found many applications in various fields, from packaging to automotive and from sports and recreation to aerospace industries (Gibson and Ashby, 1999). The widespread application of foams in the aforementioned areas is directly associated with the tailorability of their physical, thermal, and mechanical properties achievable through microstructural modifications. Like other classes of engineering materials, the microstructural attributes in foams play pivotal roles in governing their macroscopic behavior (Saha et al., 2005). Consequently, revealing the correlations between the microstructure and macroscale properties of foams has been an exciting research topic for decades.

Correlating the mechanical behavior of foams at micro and macroscopic scales requires a systematic characterization at the two length scales. Therefore, it is imperative first to define the physical dimensions that separate the two length scales. As such, identifying the transitional length scale between micro and macroscopic behavior in foams is of crucial significance (Jung et al., 2019). From computational modeling and micromechanics perspectives, it is at the so-called transitional length scales (also referred to as mesoscale (Bici et al., 2017; Sun et al., 2017)) that the homogenization of the microscopic response will lead to a meaningful macroscopic behavior (Settgast et al., 2020; Hardenacke and Hohe, 2009). From a material characterization standpoint, the physical dimensions of a foam test piece must be larger than the transitional length scale so that the measured response of the test piece is representative of the macroscopic behavior (Tekoglu et al., 2011; Zhang et al., 2019; Koohbor et al., 2020a).

Considering the significance of composite materials in practice, the nature, geometric characteristics, and physical dimensions of the micro-macro transitional length scale have been investigated in various classes of heterogeneous materials using different approaches. Most recent research works conducted in this area have been focused on the characterization of the transitional length scales in various types of composites. As such, several computational and experimental approaches have been established to characterize the effects of reinforcement type, loading conditions, internal damage, etc., on the physical dimensions of the transitional length scale in composites (Koohbor et al., 2017; Swaminathan et al., 2006; Firooz et al., 2019; Tian et al., 2015). Regardless of the method of characterization (computational, analytical, or experimental), it has been common to quantify the physical dimensions of the transitional length scale in terms of the number of inclusions in

* Corresponding author.
E-mail address: koohbor@rowan.edu (B. Koohbor).

https://doi.org/10.1016/j.mechmat.2021.104006
Received 14 May 2021; Received in revised form 19 July 2021; Accepted 30 July 2021
Available online 3 August 2021

heterogeneous materials. For instance, the transitional length scale at which the homogenization of microscale behavior leads to the macroscopic mechanical response in fiber composites has been reported as 2D domains that contains at least 50 randomly oriented fiber cross-sections (Swaminathan et al., 2006). Model predictions suggest that the transitional length scale in fiber composites can be enlarged by 2–3 times when internal damage is introduced to the microstructure (Swaminathan and Ghosh, 2006). The micro-macro transitional length scale, sometimes interchangeably used as the material's representative volume element (RVE), has been studied in other classes of materials as well (e.g., in metals and alloys (Efstathiou et al., 2010; Ravindran et al., 2017; Vieira et al., 2021)). RVE sizes identified for polycrystalline metallic samples range from domains that encompass 27 to ~700 grains (Ravindran et al., 2017).

Accurate quantification of the physical length scale at which the mechanical behavior of a foam deviates from micromechanics to macroscopic response is also of great significance, as is the case in other classes of engineering materials. This characteristic length scale is especially important in multiscale characterization and high-fidelity modeling of foams (Marvi-Mashhadi et al., 2020; Shrimali et al., 2020; Ghazi et al., 2019). Despite its importance, research studies that aim to identify micro-to-macroscale transition length scale in foams are scarce and mostly limited to pure computational studies with no experimental verifications (Alsayednoor and Harrison, 2016; Alsayednoor et al., 2013; Brun et al., 2009; Cho et al., 2017; Iasiello et al., 2019; Doskar and Novak, 2016; Kanaun and Tkachenko, 2007). Furthermore, the results obtained from these modeling works are scattered and inconclusive when compared with the few experimental works available (Brun et al., 2009). For example, modeling analyses conducted by Alsayednoor et al. (2013) on 2D periodic cellular structures with controlled levels of cell shape irregularities suggest that the RVE must contain >2400 cells for a completely strain-independent response. On the other hand, experimental findings by Brun et al. (2009) suggest RVE sizes that are approximately 2 orders of magnitude smaller than those predicted by numerical modeling.

Recent advancements in experimental strain measurements by digital image correlation (DIC) have made it possible to investigate the multiscale deformation response of heterogeneous materials in various loadings conditions (Koohbor et al., 2018a, 2018b; Tracy et al., 2015). These analyses include but are not limited to micromechanics and failure characterization in fiber composites and rigid foams in quasi-static and dynamic loading conditions. When combined with statistical analyses, DIC has also shown promising potential in identifying the micro-to-macro transition length scale in heterogeneous materials (Koohbor et al., 2017, 2018c; Mehdikhani et al., 2020). In light of all preceding background, the present work is focused on the introduction and implementation of a combined experimental-statistical approach that is utilized to characterize the transitional length scale in polymeric foams. The proposed approach is based on a statistical algorithm that compares the measured strain values at micro and macro scales. The convergence between the global (macro) and local microscopic strain fields averaged over a precisely defined 2D domain is used as a quantitative metric for the so-called transitional length scale. The potentials of the approach discussed in this work in the area of polymeric foams have not been fully explored yet, despite the validation of its accuracy for the case of fiber composites and crystalline metals (Koohbor et al., 2017; Ravindran et al., 2017). Therefore, the present study investigates the multiscale mechanics of polymeric foams with a specific focus on determining the physical dimensions that separate micro and macroscopic deformation behaviors. The specific questions that the present study will address are: (1) How can experimental strain measurements at various length scales be correlated? (2) How can multiscale full-field strain measurements be used to separate macroscopic with micro/-mesoscale behaviors? (3) How can such multiscale measurements be used to identify RVE lengths scale in foams? (4) How does RVE size in foams vary with density?

2. Materials and methods

2.1. Materials and sample preparation

Elastomeric polyurea foams with nominal densities of 100 and 214 kg m^{-3} were utilized in this work (Youssef and Reed, 2021). The selection of polyurea foam is based on two symbiotic motivations. First, polyurea has been systematically studied over the past two decades, showing superior impact mitigation, chemical and moisture resistance, and mechanical properties (Youssef and Whitten, 2017; Youssef et al., 2018). Second, the foam inherited the intrinsic characteristics of bulk polyurea while exhibiting a unique response due to its semi-closed cell structure and tailorable properties. The cell structure and macroscopic mechanical response of the polyurea foams were characterized in recent studies (Reed et al., 2019; Youssef et al., 2020; Do et al., 2019; Youssef et al., 2021). As illustrated in Fig. 1, the microstructure of the examined foams consists of spherical cells with average cell diameters ($\bar{d}$) of 302.3 ± 91.3 and 148.9 ± 70.4 μm for the low and high density foams, respectively, which were found to be in good agreement with those previously reported (Reed et al., 2019; Youssef et al., 2020; Do et al., 2020). The cellular characteristics of the higher density foam are exemplified by average cell size, roughly half of that of the low-density counterpart. However, the cell size variability in the high-density foam is significantly higher than the low-density foam samples used in this work. It is also worth noting that a close examination and analysis of SEM micrographs demonstrates the hierarchical structure of these foams with perforations randomly distributed on the surface of each spherical unit cell. Another striking feature of polyurea foams discussed here is the nucleation and deposition of microspheres on the inner surface of the unit cell, regardless of the density, which is attributed to the violent mixing process (Youssef and Reed, 2021). Do et al. (2020) quantified the percent perforation in low-density and high-density foams, resulting in ~40 % difference in the perforated surface area while being directionally unbiased. The reinforcing polyurea microspheres were found to have minimal results on the macroscale and microscale deformations, not influencing the deformation state, as discussed later.

Cubic samples of 20 × 20 × 20 mm dimensions were punched out from larger foam slabs using a hydraulic press. The punching process was selected over razor blade cutting to produce a consistent surface finish with straight edges suitable for the DIC investigation utilized herein. During the sample extraction, the sample punching using the hydraulic press was done at moderate ram speeds to avoid barreling or the hour-glass effect. It is important to note that the hot wire method was avoided to prevent sealing the cells shut due to the thermoset nature of polyurea. The above sample dimensions were selected to ensure that the cubic test pieces would contain at least 130,000 cells. This number is roughly 50 times higher than those reported in (Alsayednoor and Harrison, 2016) for the number of cells required to eliminate the sample size effect in generic cellular structures. Due to the near-perfect spherical shape of the cells in each foam, it was assumed that the mechanical response of the foams is isotropic (Youssef et al., 2021).

2.2. Mechanical testing and multiscale DIC

DIC was used to characterize strain fields developed on the surface of the foam samples at two length scales. For macroscale DIC measurements, the natural surface features (cell geometry and solid cell walls) on the camera-facing surface of the sample were used for subset tracking and strain field determination (Felten et al., 2020; Koumlis and Lamberson, 2019). The surface of interest was also coated with a thin layer of black paint to increase the contrast and improve the image correlation quality at the macroscale. Fig. 2a shows the front surface of the foam samples used for macroscale DIC. The combination of the black paint and the natural cellular features of the sample was sufficient for DIC measurements at the macroscopic scale.

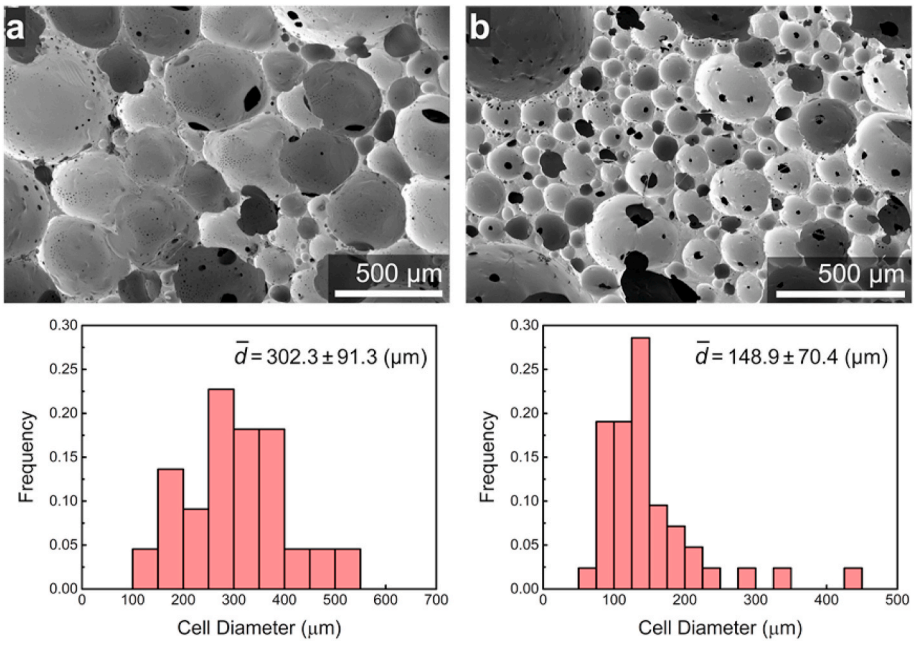

Fig. 1. SEM micrographs of the examined polyurea foams with (a) 100 and (b) 214 kg m^{-3} nominal densities. A cell size histogram for each density variation is shown below its micrograph. The histograms show the cell size variation of the SEM images shown in (a) and (b).

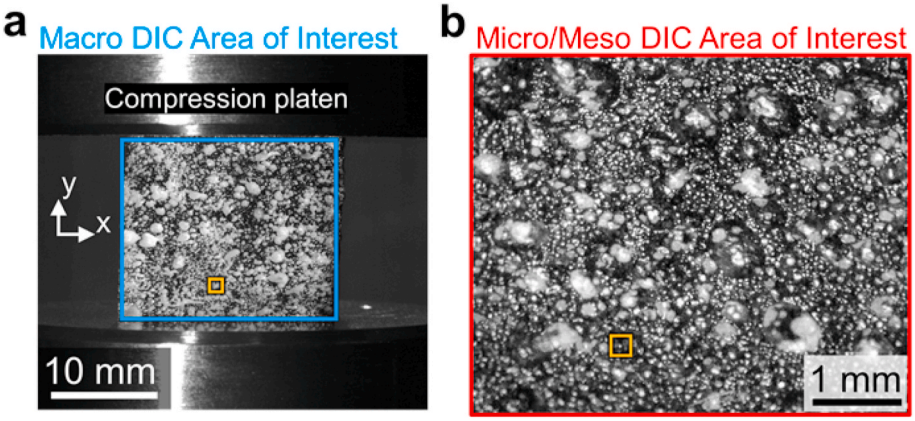

Fig. 2. DIC areas of interest for (a) macroscale and (b) micro/mesoscale strain measurements. Corresponding subset sizes are shown by overlaid yellow squares in each case. Grayscale images are from the low-density samples. (For interpretation of the references to color in this figure legend, the reader is referred to the Web version of this article.)

Foam samples were subjected to uniaxial compressive loads applied at a rate of 1 mm min^{-1}, equivalent to a nominal strain rate of 8×10^{-4} s^{-1}. The applied compressive force was measured at a rate of 1 Hz. During loading, images were captured from the front surface of the sample at a rate of 1 Hz. Images were recorded using a 5 megapixel monochromatic camera equipped with a 50 mm lens. Loading and imaging continued until the foam samples reached global densification strains. Images captured during testing were analyzed in the image correlation software Vic-2D (Correlated Solutions, Inc.) using subset and step sizes of 1.12 mm (29 pixels) and 0.27 mm (7 pixels), respectively. Strain fields were determined using a virtual strain gauge (strain filter × step size) of 1.35 mm for macroscale strain mapping. The strain noise floor associated with the utilized image correlation parameters was determined as 23×10^{-4} using the approach detailed in (Koohbor et al., 2016, 2017). DIC results were validated by comparing the engineering strain values measured by macroscale DIC and the compression platen displacements.

Strain fields were also measured at micro/mesoscales using the same approach but through independent measurements. For small-scale measurements, the same sample dimensions (i.e., 20 × 20 × 20 mm) were utilized; however, image acquisition was conducted at significantly smaller areas of interest. For this purpose, the camera was equipped with high magnification lenses that enabled imaging at areas of interest as small as 5000 × 4000 μm^2. The random distribution of cells provided enough contrast for successful image correlation analyses at small scales (see Fig. 2b). For micro/mesoscale measurements, the subset and step sizes of 207 μm (29 pixels) and 50 μm (7 pixels) were used. The virtual strain gauge size used at small scales was determined to be 250 μm. The utilized virtual strain gauge size was small enough to enable strain measurements at dimensions on the cell size order in the examined materials. The strain noise floor for small-scale DIC was determined to be 45×10^{-4}. Image acquisition in small-scale measurements was halted at the onset of local densification. More discussions on the local densification behavior of the samples are provided in the forthcoming sections.

2.3. Definition of deformation metrics

Before embarking on reporting and discussing the results, defining the metrics used in multiscale deformation characterizations is necessary. Fig. 3 shows the schematic representation of various strain metrics used in the present study. The global mechanical behavior of the foam samples was investigated using the definitions of engineering (nominal) stress and strain. Engineering stress, S, is defined simply as the compressive load, P, divided by the original cross-sectional area of the foam test piece. Engineering strain, e, is expressed as the ratio between the change of sample height, Δl, and the original height, l_0. Engineering strain indicates the average nominal strain over the sample height and; thus, it does not carry local deformation data developed due to material heterogeneity.

Two additional strain metrics were also introduced and utilized to correlate the deformation behavior at the macro and micro/mesoscale. Denoted by ε_{macro}, true strains applied at macroscale were defined as the average of all local axial strain components measured over the entire area of interest at macroscales. The number of data points used to evaluate this parameter depends on the DIC data density, which is a function of the area of interest (i.e., 20 × 20 mm^2 as shown in Fig. 2a), the subset, and step sizes. The last strain metric used to evaluate the strain development at smaller length scales is denoted by $\bar{\varepsilon}_{micro}$. This parameter is the arithmetic average of all local strain data that falls inside an R × R averaging box. Therefore, $\bar{\varepsilon}_{micro}$ is a function of the averaging box size. The concept of box averaging is discussed in Sec. 3.1.

3. Characterization of micro-to-macro transition scale

3.1. Box-averaging approach

The micro-to-macro transition scale in this work refers to a planar domain, wherein the homogenization of microscale strains will be equal to the macroscale strain. In that sense, the transition length scale can be regarded as the RVE size as well. A box-averaging approach was implemented to determine the physical size of the planar domain. Similar box-averaging techniques have been used in previous studies to characterize the RVE size in various material systems (Koohbor et al., 2017; Mehdikhani et al., 2020; Youssef et al., 2021). The schematic representation of the box-averaging process is shown in Fig. 4. In this approach, full-field strain maps at small scales are first determined by DIC. The numerical values of the local strain data are then imported into a MATLAB® script as 2D arrays. The number of data points and the physical dimensions of the DIC maps are also known and used as inputs. A virtual R × R μm^2 square box is then placed at the center of the 2D local strain array. Next, the arithmetic average of all local strain data that fall inside this box is calculated. The box-averaged strain, $\bar{\varepsilon}_{micro}$, is

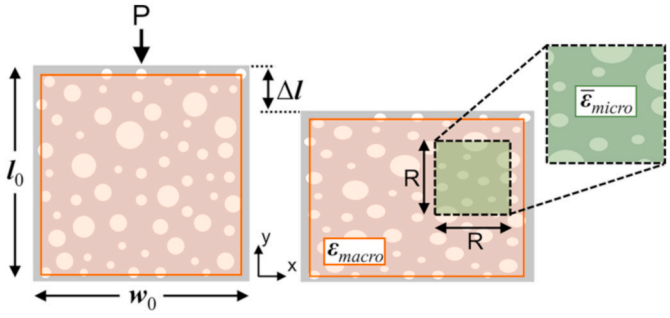

Fig. 3. Schematic representation of various strain metrics used in this work. Engineering strain is defined as e = Δl/l_0. ε_{macro} is defined as the average of local axial strain components inside the red box. $\bar{\varepsilon}_{micro}$ is defined as the average of all local axial strain data inside a smaller R × R averaging box highlighted by green color. (For interpretation of the references to color in this figure legend, the reader is referred to the Web version of this article.)

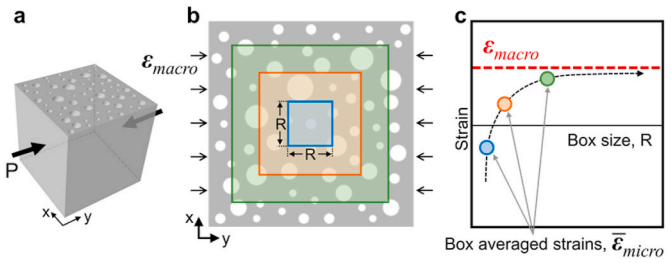

Fig. 4. Schematic representation of the box averaging algorithm used to identify the transitional length scale in the examined foams: (a) A cubic foam sample subjected to axial compression that leads to a macroscopic strain, ε_{macro}. (b) The progressive increase of the averaging box in which the homogenization of local strains is performed. (c) Convergence between macroscopic and box-averaged microscale strains enables the identification of the transition length scale.

then compared with ε_{macro}. The quantitative comparison between the two metrics for given box size, R, is established by using Equation (1):

$$\delta(R) = \frac{\varepsilon_{macro} - \bar{\varepsilon}_{micro}(R)}{\varepsilon_{macro}} \times 100 \quad (1)$$

wherein, δ(R) is a unitless parameter used to quantify the convergence of macroscale and averaged microscale strains. The size of the averaging box is incrementally enlarged, and the above process is repeated until the convergence criterion is satisfied. To be consistent with previous studies, the convergence criterion in the present study was chosen as $|\delta| \leq 2.5\%$ (Koohbor et al., 2017; Swaminathan et al., 2006; Brun et al., 2009; Ren and Zheng, 2002). The averaging box size that satisfies the convergence criterion is identified as the micro-to-macro transition length scale for a given engineering strain. The same process is iterated at different strains and for the two different foam densities. Note that the choice of a squared averaging box in this work was solely due to the convenience in the development of the computer code. Since all characterizations discussed herein are based on a spatial averaging approach, we are convinced that the shape of the averaging box will have a minimal effect on the results.

3.2. Validating location-independence of box-averaging approach

The transition length identification process, described in Sec. 3.1, must be independent of the initial location of the averaging box (Swaminathan et al., 2006). Therefore, five different starting points were considered to confirm the location-independence of the box averaging approach. As shown in Fig. 5, the initial locations of the smallest averaging box were selected to be at the center (CTR), upper left (UL), upper right (UR), lower left (LL), and lower right (LR) of the strain measurement area. The process outlines in Sec. 3.1. was then implemented for each box location. It should be noted that the smallest box size in each case is equal to the spacing between two adjacent data points in the small scale DIC analyses. This spacing is equal to the step (subset shift) size, i.e., 50 μm. The size of the largest averaging box was determined by the vertical dimension of the micro/meso DIC area of interest, which was 4000 μm.

4. Results and discussions

4.1. Macroscale behavior and global densification

Macroscopic mechanical behaviors of the foams were studied in quasi-static compression. Fig. 6 shows the stress-strain curves obtained for each density variation of polyurea foam at a strain rate of 8 × 10^{-4} s^{-1}. Stress-strain behaviors of the foam samples in this work are typical of other elastomeric foams, wherein an initial linear trend in the small deformation region changes into nonlinear hardening behavior at larger

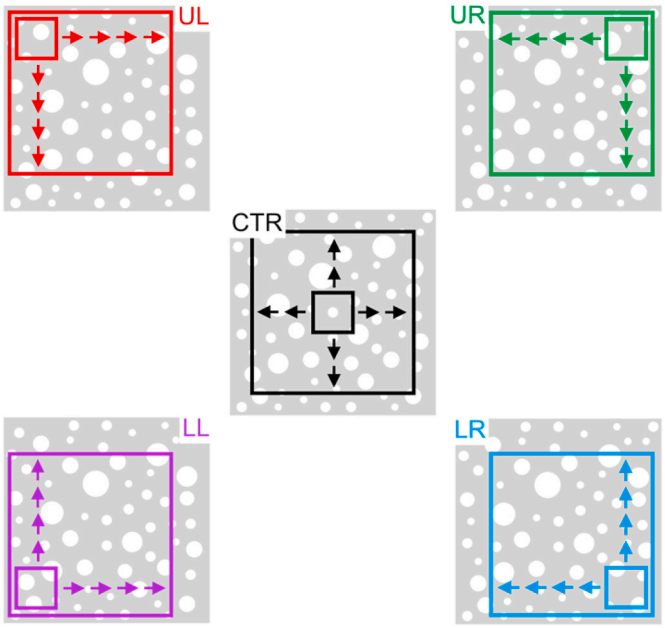

Fig. 5. Schematic of the initial box locations used for validating location independence of the box averaging approach. The initial box location in each case is marked by uppercase letters, CTR (center), UL (upper left), UR (upper right), LL (lower left), LR (lower right). The arrows indicate the continuous enlargement of the averaging box from its initial location until it covers the entire area of interest.

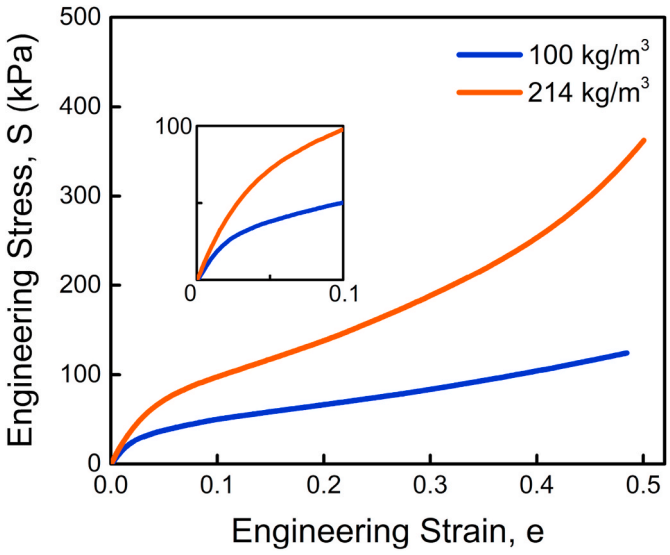

Fig. 6. Engineering stress-strain response of the examined foams in compression. Compression tests were performed at a nominal strain rate of 8×10^{-4} s^{-1}.

strains. The nonlinear behavior is due to a reversible densification effect which stems from gradual buckling and collapse of the cell structure in response to the applied compressive load. The slopes of the linear regions of the curves were quantified as 1.54 MPa and 2.31 MPa for the low and high density foams, respectively. The stress and strain limits of the linear regions were determined using a 0.2 % offset method (Koohbor et al., 2020b). Accordingly, the onsets of nonlinear elastic response for the low and high density foams were measured to be 19.5 kPa and 35.7 kPa, respectively. Nominal strains corresponding to these stress levels were ~0.015 for both samples.

Global densification strain for each sample was characterized as the strain magnitude at which maximum efficiency is obtained. The efficiency parameter, η, is defined as the ratio between the strain energy absorbed by the foam at a certain strain and the stress at the same strain level, i.e.,

$$\eta(e) = \frac{\int_0^e S.de}{S(e)} \tag{2}$$

Consistent with previous studies (Uddin et al., 2020), global densification for both samples were found to occur at engineering strains of ca. 0.47.

4.2. Micro and macroscale strain fields

Fig. 7 shows the evolution of axial strain fields (ε_{yy}) at macro and microscales at various stress and strain levels for the low-density variation of the foam. The heterogeneous strain distribution in both cases originates from the non-uniform deformation and collapse of cells in the microstructure, manifested by the development of banded strain patterns. The intensity of the strain heterogeneity is more pronounced in the small-scale measurements. The higher degrees of strain heterogeneity at smaller length scales are exemplified by the narrow regions of high strain bands that form inside and span laterally across the DIC area of interest. It is interesting to note that although global (macro) densification in the examined foams occurs at nominal (engineering) strains of ~0.47, the formation of the highly compressed bands revealed at small scales indicates that the densification process in foam samples is gradual and initiates locally at strains significantly smaller than those associated with global densification. A similar general response was observed for the high-density foam as well.

While general similarities between the deformation responses of the samples were observed, the degree of small-scale strain heterogeneity was found to be different for the two foam densities. Fig. 8 shows the distribution of local strain at microscales extracted along the vertical axis of the DIC area of interest. In both foam samples, the local strain response shows a pseudo-periodic pattern. The degree of oscillations is more consistent for the low density foam (Fig. 8a). Besides, the range of local strains variation (i.e., $\Delta\varepsilon_{micro} = \varepsilon_{micro}^{max} - \varepsilon_{micro}^{min}$) is higher for the high density foam. For example, considering the data presented in Fig. 8, the range of local strain variation (at an engineering strain of e = 0.092) for the low and high density foams is calculated as 0.34 and 0.45, respectively. The larger cell size variability in the higher density foam sample (see Fig. 1) is likely associated with this behavior.

Tracking the evolution of the Poisson's ratio in elastomeric foams was previously reported as a metric that enables the characterization of various deformation stages (Koohbor et al., 2020b). As such, the Poisson's ratios of the foam samples in the present study were measured using the in-plane strain fields obtained from macroscale DIC. The Poisson's ratio of each density variation of the foam was measured as the numerical derivative of the lateral, ε_{xx}, with respect to the axial, ε_{yy}, strain components. Fig. 9 shows the evolution of Poisson's ratio of the

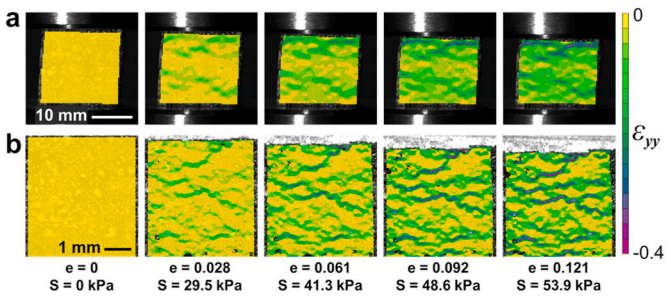

Fig. 7. Distribution of axial strain fields at (a) macro and (b) micro/meso DIC areas of interest at various engineering strain, e, and stress, S, levels for the low density foam. Compressive load is applied vertically.

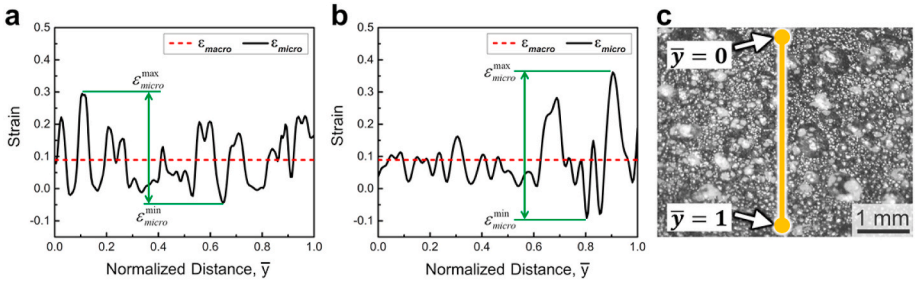

Fig. 8. Variation of local (micro) strain for (a) low density and (b) high density foam samples at an engineering strain of e = 0.092. Local strain data are plotted with respect to normalized vertical coordinates, $\bar{y}$, shown in (c).

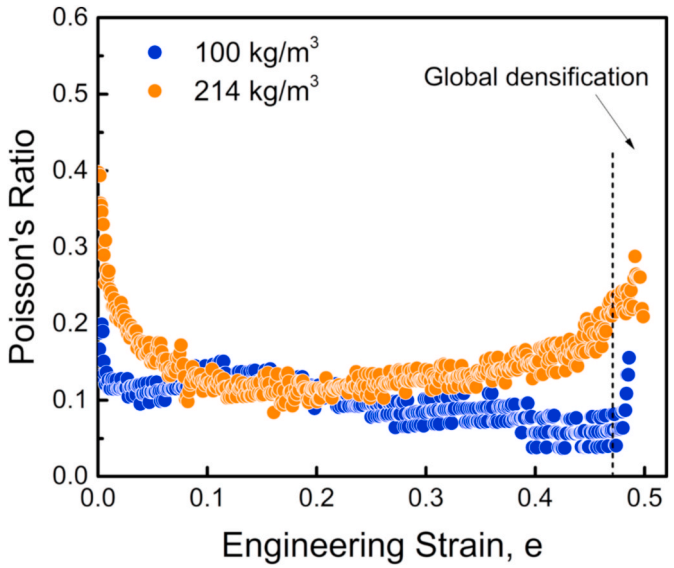

Fig. 9. Evolution of the Poisson's ratio of the foam samples with engineering strain. Nominal strains associated with the onset of non-linear elastic and global densification are marked by dashed lines.

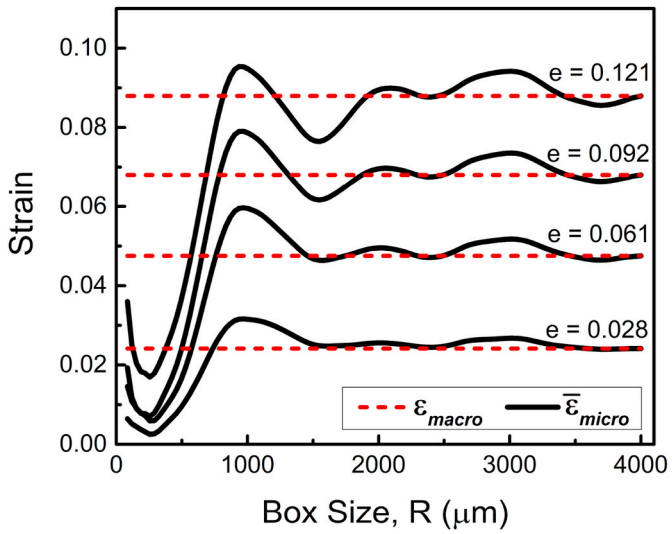

Fig. 10. Variation of box-averaged strain, $\bar{\varepsilon}_{micro}$, with respect to box size, R, at various engineering strains for the lower density foam. Dashed lines represent ε_{macro}. Data obtained from the low density foam.

foam samples with engineering strain. In both foam cases, the Poisson's ratio is found to decrease rapidly as the global strain is increased. Upon passing e = 0.015 (i.e., the onset of nonlinear deformation), the variation of the Poisson's ratio reaches a plateau. In the nonlinear deformation region, the Poisson's ratios of the foam samples remain nearly constant and at ~0.1. At larger deformations, the Poisson's ratio tends to increase slowly but steadily in the higher density foam while slightly decreasing in the low-density samples. Upon passing through the global densification strain, both curves show a rapid increase, resulting from a complete collapse of the cells in the foam. At strains beyond global densification, the mechanical deformation of the foam resembles that of nonporous, bulk elastomeric solid subjected to large deformations. Considering the strain patterns and Poisson's ratio evolution, it is evident that the deformation behavior of the examined foams varies most significantly over an engineering strain range of e = 0 to ~0.15. Besides, the relatively low Poisson's ratios over this strain range (especially at e > 0.015) limit the out-of-plane motion, leading to a more accurate assessment of the full-field deformation response using 2D DIC (Sutton et al., 2008). Therefore, the transition length scale characterization and the relevant box averaging approaches will be investigated in this range.

4.3. Correlating micro and macroscale deformations

Fig. 10 shows the variation of box-averaged strains with respect to the box size at different nominal strain values for the low-density foam. The curves shown in this figure are obtained using the CTR averaging box (see Fig. 5). At smaller R values, the box-averaged strains show high amplitude fluctuations around the corresponding macroscopic strains. The oscillations in $\bar{\varepsilon}_{micro}$ decay as the size of the averaging box increases. The two strain metrics, $\bar{\varepsilon}_{micro}$ and ε_{macro}, converge as the averaging box size increases above ca. 3500 μm. The differences between the values of engineering and macroscopic strain metrics in Fig. 10 stem from (1) the basic definitions (i.e., logarithmic and simple fraction) of the two metrics that lead to larger divergence at higher strains, and (2) the significant contribution of the local strain heterogeneities that are included in the macroscopic strain metric but not in the engineering strain.

The data shown in Fig. 10 can be used as input to Equation (1) to enable a quantitative determination of the micro-to-macro transition scale. However, before doing so, the location-independence of the box averaging approach must be validated. This validation is shown in Fig. 11, wherein the variation of box-averaged strains versus box size is shown for various initial box locations described in Sec. 3.2. The trends indicate large oscillations, due to strain localization at the cell level, at small box sizes that tend to decay at larger box sizes, leading to convergence at R > 3500 μm.

After confirming the location-independence of the box-averaging approach, it is now possible to establish a quantitative correlation between small-scale and macroscale deformation behaviors in the examined foams. To this purpose, the variation of the convergence parameter, δ, was plotted against the box size in various strains and for both foam samples. As illustrated in Fig. 12, δ-R curves for both foam densities show consistent overall trends. In both samples, the curves show high

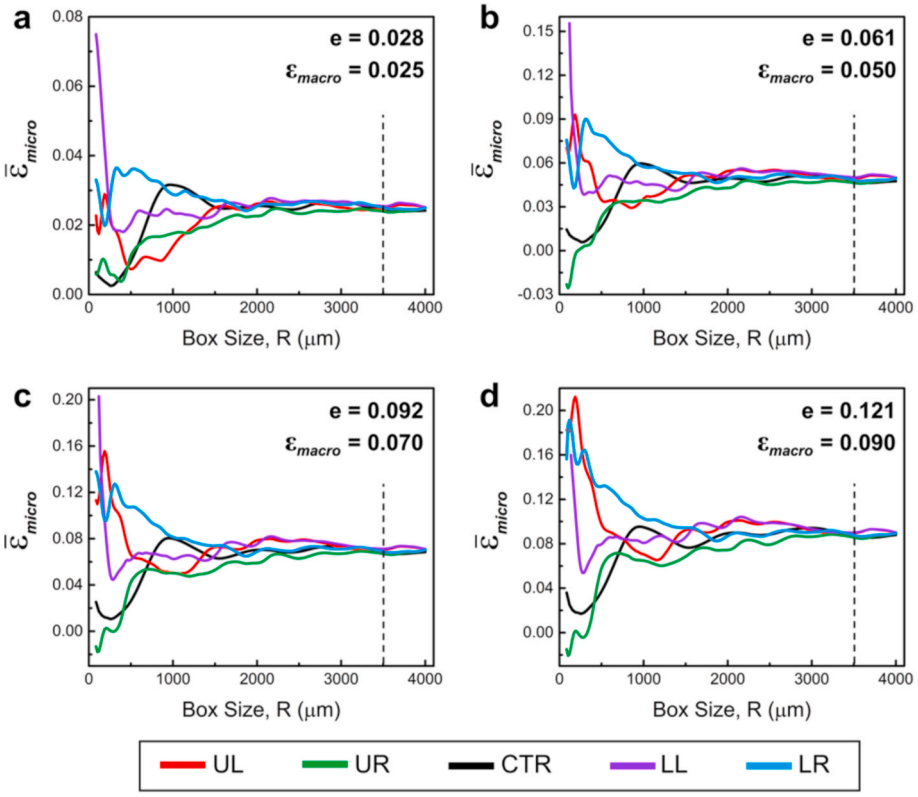

Fig. 11. Variation of box-averaged strains ($\bar{\varepsilon}_{micro}$) versus box size for different initial box locations. Data obtained from the low density foam. Vertical dashed lines mark the R = 3500 μm threshold.

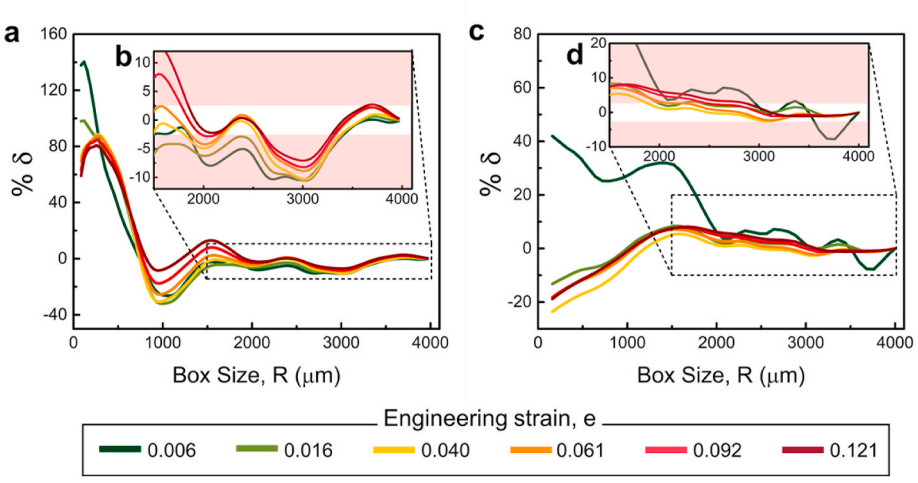

Fig. 12. Convergence parameter, δ, plotted against averaging box size, R, at various engineering strains for (a) low density, and (c) high density foam samples. Insets marked by (b) and (d) are the close-up view of the graph showing the region where the convergence criterion is satisfied (unshaded).

amplitude variations at small box sizes. The oscillations quickly decay at larger R values. The convergence criterion (i.e., $|\delta| \leq 2.5\%$) is met at R > 3500 μm and R > 2800 μm for the low and high density foams, respectively, in part due to the difference in the cell size.

The R sizes at which the convergence criterion was met were identified for both foam densities at different global engineering strain magnitudes and different initial box locations (see Fig. 5). Here, R_T denotes the R sizes that satisfied the convergence criterion, where the value R_T is a measure for the micro-to-macro transition length scale. Fig. 13 shows the variation of this parameter at different global strains and for both foam densities. The scatter bars in this figure represent the variability of identified R_T values for different initial box locations. Compared with the low-density foam, the R_T values variability is generally higher for the high-density samples. This behavior may be related to the higher degree of local strain heterogeneity, which is, in turn, associated with the larger cell size variability in the higher density foam (see Fig. 8). Nonetheless, the R_T values variability decreases at larger strains for both foam densities, consistent with previous experimental works and relates to high noise to strain ratios at small strain conditions (Koohbor et al., 2017). Furthermore, the average values of the identified transition length scales are independent of strain, at least over a strain (e) range of 0.03–0.12. The strain independence of the

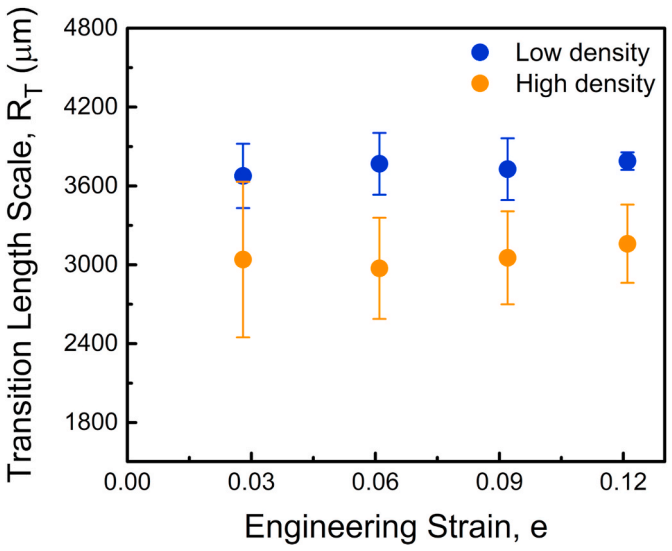

Fig. 13. Transition length scale, R_T, versus engineering strain for low and high density foam samples. Scatter bars represent the variability of R_T values across different initial box locations.

transition length scales is in agreement with the fundamental definition of the RVE by Hill (1963), which states that the RVE size must be "effectively independent of the surface values of traction and displacement." Therefore, it is reasonable to assume that the transition length scales identified herein can be used as a measure for the RVE size of the examined foams. However, it must be emphasized that because 2D DIC measurements were used as the basis for the analyses in this work, the transition length scales can be thought of as representative surface elements (RSE) and not volumetric elements (Efstathiou et al., 2010). While there still exists no universal approach to correlate RSE and RVE, the isotropic mechanical behavior of the examined foams that originates from the symmetry and randomness of the materials' cell structure allows us to assume that the transition length scales reported here are equivalent to the RVE size of the foams.

4.4. Effects of density and cell size

Correlations between the transitional length scale, R_T, and the cell size/number can be established for different foam densities. To do so, the average number of cells per unit length, N_c, for each foam density is determined first. This quantity has been characterized for each foam by averaging at least ten independent measurements performed using straight lines oriented at arbitrary angles applied on the SEM micrographs shown in Fig. 1 (Gibson and Ashby, 1999). The N_c values were 3.45 ± 0.68 and 6.31 ± 1.40 cells per 1000 μm for the low and high density foams, respectively. Comparing R_T and N_c values for each foam density, the number of cells per axis required to represent macroscale response is 13.02 ± 2.54 and 19.28 ± 4.28 for the low and high density foams, respectively. Finally, translating these values into the three-dimensional space, it is concluded that the smallest volume element to represent the macroscopic response of the material must contain at least 3700 and 13,000 cells for the low density and high density foam samples, respectively. It is interesting to note that the ratio between minimum cell numbers reported here is not directly proportional to the ratio of the foams' densities. While it is expected that the foam density (which is directly correlated with the solid fraction in the foam) will have a significant effect on the RVE size of a material, we also believe that the larger cell size variability is a major contributing factor in the large variations in the identified RVE dimensions. As discussed in the previous sections (see Fig. 8), the higher degrees of cell size variability in the high density foam may be directly related to the more significant strain heterogeneity in this sample.

Another noteworthy observation in the present work is that the identified RVE sizes fall between those characterized by Brun et al. (2009) for fluid flow properties and those in Alsayednoor et al. (2013) evaluated numerically for 2D hexagonal geometries. Unlike these previous studies, the analyses presented in the current work were based on pure experimental measurements and, thus, contain the inherent sources of heterogeneity in the material as well as the deformation fields. The latter may be the primary source of discrepancy between the RVE sizes identified in this work and those determined previously by numerical analyses. In particular, studies in which RVE size determination is conducted by modulus measurement (e.g., Kanit et al., 2003; Swaminathan et al., 2006) often do not incorporate the stochastic nature of deformation heterogeneity due to material/geometric inconsistencies. Therefore, such modulus-based RVE size determination approaches tend to underestimate the RVE sizes in highly heterogeneous structures. The inclusion of such inherent deformation heterogeneities in the present work can be considered a unique contribution in the field of multiscale characterization of porous structures. Besides, from an application standpoint, the findings of the present work can provide practical guidelines to experimental studies that are sensitive to sample size (e.g., impact loading of foam and other porous structures wherein the developed inertia stresses are directly proportional to sample size (Song et al., 2019; Koohbor et al., 2020a)). Moreover, the outcomes of this research can be beneficial for studies that utilize spatial strain averaging for characterizing the constitutive response of foams and other cellular structure (e.g., parameter identification studies by virtual fields method (Wang et al., 2016)).

5. Conclusions

A multiscale full-field strain measurement approach was proposed to identify the length scale at which a transition from micro to macroscale mechanics occurs in polymeric foams. The implemented methodology was based on correlating macroscopic strain fields with those developed at micro/mesoscales facilitated by a statistical approach. The statistical approach used the spatial averaging of local strain data within 2D squared domains referred to as an averaging box. The strain and density dependence of the box averaging approach were investigated. The analyses suggest that the utilized statistical approach makes it possible to correlate experimentally measured strain fields at various length scales. More importantly, such multiscale characterization techniques can be utilized to separate the length scales at which macro and micromechanics behaviors begin to diverge. The scales at which such divergence occurs sets the micro-to-macro transitional length scale and can be regarded as a measure for the RVE dimensions of the material. The latter was further studied by validating the strain-independence of the box averaging approach. Finally, the transitional length scales were found to be density-dependent but independent of the global strain in polymeric foams. The density-dependence was correlated with the average size and number of the cells in the examined foams.

Credit author statement

Behrad Koohbor: Conceptualization, Methodology, Formal Analysis, Writing-Review & Editing, Funding Acquisition. Nicholas Pagliocca: Methodology, Investigation, Writing-Original draft preparation. George Youssef: Conceptualization, Supervision, Writing-Review & Editing, Funding Acquisition

Data availability

Data will be available upon request.

Declaration of competing interest

The authors declare that they have no known competing financial interests or personal relationships that could have appeared to influence the work reported in this paper.

Acknowledgments

This material is based upon work supported by the National Science Foundation under Grant No. 2035660 (B.K.) and Grant No. 2035663 (G. Y.). B.K. acknowledges the Advanced Materials and Manufacturing Institute (AMMI) at Rowan University for the financial support. G.Y. acknowledges the support from internal San Diego State University and the Department of Defense under Grant Agreement No. W911NF1410039 and No. W911NF1810477.

References

Alsayednoor, J., Harrison, P., 2016. Evaluating the performance of microstructure generation algorithms for 2-d foam-like representative volume elements. Mech. Mater. 98, 44–58.

Alsayednoor, J., Harrison, P., Guo, Z., 2013. Large strain compressive response of 2-D periodic representative volume element for random foam microstructures. Mech. Mater. 66, 7–20.

Bici, M., Campana, F., De Michelis, M., 2017. Mesoscale geometric modeling of cellular materials for finite element analysis. Computer-Aided Design and Applications 14, 760–769.

Brun, E., Vicente, J., Topin, F., Occelli, R., Clifton, M.J., 2009. Microstructure and transport properties of cellular materials: representative volume element. Adv. Eng. Mater. 11, 805–810.

Cho, Y.J., Lee, W., Park, Y.H., 2017. Finite element modeling of tensile deformation behaviors of iron syntactic foam with hollow glass microspheres. Materials 10, 1201.

Do, S., Rosenow, B., Reed, N., Mohammad, A., Manlulu, K., Youssef, G., 2019. Fabrication, characterization, and testing of novel polyurea foam. PU Magazine International 16 (2), 104–107.

Do, A., Huynh, N.U., Reed, N., Shaik, A.M., Nacy, S., Youssef, G., 2020. Partially-perforated self-reinforced polyurea foams. Appl. Sci. 10 (17), 5869.

Doskar, M., Novak, J., 2016. A jigsaw puzzle framework for homogenization of high porosity foams. Comput. Struct. 166, 33–41.

Efstathiou, C., Sehitoglu, H., Lambros, J., 2010. Multiscale strain measurements of plastically deforming polycrystalline titanium: role of deformation heterogeneities. Int. J. Plast. 26, 93–106.

Felten, M., Fries, M., Pullen, A., Proud, W.G., Jung, A., 2020. Investigation of strain-rate effects in Ni/PU hybrid foams under low-impact velocities. Adv. Eng. Mater. 22, 1901589.

Firooz, S., Saed, S., Chatzigeorgio, G., Meraghni, F., Steinmann, P., Javili, A., 2019. Systematic study of homogenization and the utility of circular simplified representative volume element. Math. Mech. Solid 24, 2961–2985.

Ghazi, A., Berke, P., Ehab Moustafa Kamel, K., Sonon, B., Tiago, C., Massart, T.J., 2019. Multiscale computational modelling of closed cell metallic foams with detailed microstructural morphological control. Int. J. Eng. Sci. 143, 92–114.

Gibson, L.J., Ashby, M.F., 1999. Cellular Solids – Structure and Properties, second ed. Cambridge University Press, UK.

Hardenacke, V., Hohe, J., 2009. Local probabilistic homogenization of two-dimensional model foams accounting for micro structural disorder. Int. J. Solid Struct. 46, 989–1006.

Hill, R., 1963. Elastic properties of reinforced solids: some theoretical principles. J. Mech. Phys. Solid. 11, 357–372.

Iasiello, M., Bianco, N., Chiu, W.K.S., Naso, V., 2019. Thermal conduction in open-cell metal foams: anisotropy and representative volume element. Int. J. Therm. Sci. 137, 399–409.

Jung, A., Al Majthoub, K., Jochum, C., Kirsch, S.M., Welsch, F., Seelecke, S., Diebels, S., 2019. Correlative digital image correlation and infrared thermography measurements for the investigation of the mesoscopic deformation behaviour of foams. J. Mech. Phys. Solid. 130, 165–180.

Kanaun, S., Tkachenko, O., 2007. Representative volume element and effective elastic properties of open cell foam materials with random microstructures. J. Mech. Mater. Struct. 2, 1607–1628.

Kanit, T., Forest, S., Galliet, I., Mounoury, V., Jeulin, D., 2003. Determination of the size of the representative volume element for random composites: statistical and numerical approach. Int. J. Solid Struct. 40, 3647–3679.

Koohbor, B., Kidane, A., Lu, W.-Y., Sutton, M.A., 2016. Investigation of the dynamic stress–strain response of compressible polymeric foam using a non-parametric analysis. Int. J. Impact Eng. 91, 170–182.

Koohbor, B., Ravindran, S., Kidane, A., 2017. Experimental determination of Representative Volume Element (RVE) size in woven composites. Opt Laser. Eng. 90, 59–71.

Koohbor, B., Ravindran, S., Kidane, A., 2018a. A multiscale experimental approach for correlating global and local deformation response in woven composites. Compos. Struct. 194, 328–334.

Koohbor, B., Ravindran, S., Kidane, A., 2018b. Effects of cell-wall instability and local failure on the response of closed-cell polymeric foams subjected to dynamic loading. Mech. Mater. 116, 67–76.

Koohbor, B., Montgomery, C.B., White, S.R., Sottos, N.R., 2018c. Meso-scale strain measurements in fiber reinforced composites. 33rd Technical Conference of the American Society for Composites, Seattle, WA, USA. https://doi.org/10.12783/asc33/26028. In: http://www.dpi-proceedings.com/index.php/asc33/article/view/26028.

Koohbor, B., Singh, N.K., Kidane, A., 2020a. Radial and axial inertia stresses in high strain rate deformation of polymer foams. Int. J. Mech. Sci. 181, 105679.

Koohbor, B., Blourchian, Uddin K.Z., Youssef, G., 2020b. Characterization of energy absorption and strain rate sensitivity of a novel elastomeric polyurea foam. Adv. Eng. Mater. 23 (1), 2000797.

Koumlis, S., Lamberson, L., 2019. Strain rate dependent compressive response of open cell polyurethane foam. Exp. Mech. 59, 1087–1103.

Marvi-Mashhadi, M., Lopes, C.S., Llorca, J., 2020. High fidelity simulation of the mechanical behavior of closed-cell polyurethane foams. J. Mech. Phys. Solid. 135, 103814.

Mehdikhani, M., Breite, C., Swolfs, Y., Wevers, M., Lomov, S.V., Gorbatikh, L., 2020. Combining digital image correlation with X-ray computed tomography for characterization of fiber orientation in unidirectional composites. Compos. Appl. Sci. Manuf. 142, 106234.

Ravindran, S., Koohbor, B., Kidane, A., 2017. Experimental characterization of meso-scale deformation mechanisms and the RVE size in plastically deformed carbon steel. Strain 53, e12217.

Reed, N., Huynh, N.U., Rosenow, B., Manlulu, K., Youssef, G., 2019. Synthesis and characterization of elastomeric polyurea foam. J. Appl. Polym. Sci. 137, 48839.

Ren, Z.-Y., Zheng, Q.-S., 2002. A quantitative study of minimum sizes of representative volume elements of cubic polycrystals – numerical experiments. J. Mech. Phys. Solid. 50, 881–893.

Saha, M.C., Mahfuz, H., Chacravarty, U.K., Uddin, M., Kabir, MdE., Jeelani, S., 2005. Effect of density, microstructure, and strain rate on compression behavior of polymeric foams. Mater. Sci. Eng. 406, 328–336.

Settgast, C., Hutter, G., Kuna, M., Abendroth, M., 2020. A hybrid approach to simulate the homogenized irreversible elastic–plastic deformations and damage of foams by neural networks. Int. J. Plast. 126, 102624.

Shrimali, B., Parnell, W.J., Lopez-Pamies, O., 2020. A simple explicit model constructed from a homogenization solution for the large-strain mechanical response of elastomeric syntactic foams. Int. J. Non Lin. Mech. 126, 103548.

Song, B., Sanborn, B., Lu, W.-Y., 2019. Radial inertia effects on dynamic compressive response of polymeric foam materials. Exp. Mech. 59, 17–27.

Sun, Y., Zhang, X., Shao, Z., Li, Q.M., 2017. Image-based correlation between the meso-scale structure and deformation of closed-cell foam. Mater. Sci. Eng. 688, 27–39.

Sutton, M.A., Yan, J.H., Tiwari, V., Schreier, H.W., Orteu, J.J., 2008. The effect of out-of-plane motion on 2D and 3D digital image correlation measurements. Opt Laser. Eng. 46, 746–757.

Swaminathan, S., Ghosh, S., 2006. Statistically equivalent representative volume elements for unidirectional composite microstructures: Part II – with interfacial debonding. J. Compos. Mater. 40, 605–621.

Swaminathan, S., Ghosh, S., Pagano, S.J., 2006. Statistically equivalent representative volume elements for unidirectional composite microstructures: Part I – without damage. J. Compos. Mater. 40, 583–604.

Tekoglu, C., Gibson, L.J., Pardoen, T., Onck, P.R., 2011. Size effect in foams: experiments and modeling. Prog. Mater. Sci. 56, 109–138.

Tian, W., Qi, L., Zhou, J., Liang, J., Ma, Y., 2015. Representative volume element for composites reinforced by spatially randomly distributed discontinuous fibers and its applications. Compos. Struct. 131, 366–373.

Tracy, J., Daly, S., Sevener, K., 2015. Multiscale damage characterization in continuous fiber ceramic matrix composites using digital image correlation. J. Mater. Sci. 50, 5289–5299.

Uddin, K.Z., Youssef, G., Trkov, M., Seyyedhosseinzadeh, H., Koohbor, B., 2020. Gradient optimization of multi-layered density-graded foam laminates for footwear material design. J. Biomech. 109, 109950.

Vieira, R.B., Sehitoglu, H., Lambros, J., 2021. Representative volume elements for plasticity and creep measured from high-resolution microscale strain fields. Acta Mater. 214, 117021.

Wang, P., Pierron, F., Rossi, M., Lava, P., Thomsen, O.T., 2016. Optimised experimental characterization of polymeric foam material using DIC and the virtual fields method. Strain 52, 59–79.

Youssef, G., Reed, N., 2021. Scalable manufacturing method of property-tailorable polyurea foam. U.S. Patent Application No. 16/118, 879.

Youssef, G., Whitten, I., 2017. Dynamic properties of ultraviolet-exposed polyurea. Mech. Time-Dependent Mater. 21 (3), 351–363.

Youssef, G., Brinson, J., Whitten, I., 2018. The effect of ultraviolet radiation on the hyperelastic behavior of polyurea. J. Polym. Environ. 26 (1), 183–190.

Youssef, G., Reed, N., Hyunh, N.U., Rosenow, B., Manlulu, K., 2020. Experimentally-validated predictions of impact response of polyurea foams using viscoelasticity based on bulk properties. Mech. Mater. 148, 103432.

Youssef, G., Nacy, S., Huynh, N.U., 2021. Mechanics of microspheres reinforced hollow microcells. J. Appl. Mech. 88 (4), 041009.

Zhang, Y., Jin, T., Shiqiang, L., Dong, R., Wang, Z., Lu, G., 2019. Sample size effect on the mechanical behavior of aluminum foam. Int. J. Mech. Sci. 151, 622–638.